Editors' Suggestion   Featured in Physics

Nonlinear Effects in Black Hole Ringdown

Mark Ho-Yeuk Cheung,[1] Vishal Baibhav,[2] Emanuele Berti,[1] Vitor Cardoso,[3,4]
Gregorio Carullo,[5] Roberto Cotesta,[1] Walter Del Pozzo,[6] Francisco Duque,[4] Thomas Helfer,[1]
Estuti Shukla,[7] and Kaze W. K. Wong[8]

[1]*William H. Miller III Department of Physics and Astronomy, Johns Hopkins University,*
3400 North Charles Street, Baltimore, Maryland 21218, USA
[2]*Center for Interdisciplinary Exploration and Research in Astrophysics (CIERA) and Department of Physics and Astronomy,*
Northwestern University, 1800 Sherman Ave, Evanston, Illinois 60201, USA
[3]*Niels Bohr International Academy, Niels Bohr Institute, Blegdamsvej 17, 2100 Copenhagen, Denmark*
[4]*CENTRA, Departamento de Física, Instituto Superior Técnico—IST, Universidade de Lisboa—UL,*
Avenida Rovisco Pais 1, 1049-001 Lisboa, Portugal
[5]*Theoretisch-Physikalisches Institut, Friedrich-Schiller-Universität Jena, Fröbelstieg 1, 07743 Jena, Germany*
[6]*Dipartimento di Fisica "Enrico Fermi," Università di Pisa, Pisa I-56127, Italy*
[7]*Institute for Gravitation and the Cosmos, Department of Physics, Pennsylvania State University,*
University Park, Pennsylvania 16802, USA
[8]*Center for Computational Astrophysics, Flatiron Institute, New York, New York 10010, USA*

We report evidence for nonlinear modes in the ringdown stage of the gravitational waveform produced by the merger of two comparable-mass black holes. We consider both the coalescence of black hole binaries in quasicircular orbits and high-energy, head-on black hole collisions. The presence of nonlinear modes in the numerical simulations confirms that general-relativistic nonlinearities are important and must be considered in gravitational-wave data analysis.

Introduction.—The birth of gravitational-wave (GW) astronomy [1] marks a new era in the exploration of strong-field gravity [2,3]. As the simplest macroscopic objects cloaking curvature singularities, black holes (BHs) play a special role as astrophysical laboratories to test gravity and to search for new physics [4–9]. The structure and dynamics of BHs in our Universe is well described by the two parameters (mass M and angular momentum J) characterizing the Kerr metric. In general relativity, the perturbed BHs formed in a binary merger approach a stationary state by emitting GWs in a discrete set of characteristic quasinormal modes (QNMs) with complex frequencies determined only by M and J. The "black hole spectroscopy" program consists in observing these "ringdown" waves, measuring the QNM frequencies, using them to estimate mass and spin [10], and (if more than one mode can be observed) test that the remnant is indeed consistent with a Kerr BH [11–15]. The observability of QNMs depends crucially on their excitation in the merger process. Even within linear perturbation theory, where one only considers linear metric perturbations to Einstein's equations in the Kerr background, determining which modes are excited is a formidable problem [16–25].

General relativity is an intrinsically nonlinear theory. The merger of two comparable-mass BHs leading to a perturbed Kerr BH is one of the most violent processes in the Universe, where these nonlinearities should play an important role. It is therefore surprising that merger simulations in numerical relativity result in a very smooth transition from inspiral to merger and ringdown [26,27]. Where are the nonlinearities of general relativity?

This state of affairs has led many (including some of us) to conjecture that nonlinear effects may be hidden behind the horizon, suppressed by the presence of a photonsphere, or even absent altogether (see e.g., [28–37] and references therein). In this Letter, we show that merger simulations of BH binaries of comparable masses in quasicircular orbits (as well as high-energy, head-on BH collisions) do, in fact, excite nonlinear modes in the ringdown stage.

Second-order quasinormal modes.—In BH perturbation theory, the GW strain and the Newman-Penrose scalar Ψ_4 produced by a BH merger at late times can be approximated by a linear combination of damped sinusoids (in addition to a subdominant power-law tail as well as retrograde QNMs, which we disregard here) [14–17],

$$rh^{(1)}(t,\theta,\phi) = \sum_{n\ell m} A_{n\ell m} e^{-i(\omega_{n\ell m}t + \phi_{n\ell m})} S_{\ell m}, \quad (1)$$

where r is the (luminosity) distance from the source. The spin-2 spin-weighted spheroidal harmonics $S_{\ell m} = S_{\ell m}(\theta, \phi, \chi\omega_{n\ell m})$ depend on the angular variables (θ, ϕ), on the complex QNM frequencies $\omega_{n\ell m}$, and on the

dimensionless spin $\chi = J/M^2$ of the remnant BH [38]. This expression, found by solving the Teukolsky equation [39], is valid when the GW amplitude is small enough that one can linearize Einstein's equations in the Kerr background.

At second order in the GW amplitude one finds similar equations for the second-order perturbations $h^{(2)}$, now sourced by first-order quantities [40–47]. Let k be a generic mode, which can be either a first-order mode ($k = k_i = \ell_i m_i n_i$) or a higher-order mode. We will denote a second-order mode sourced by the first-order modes $k_1 = \ell_1 m_1 n_1$ and $k_2 = \ell_2 m_2 n_2$ as $k = k_1 \times k_2 = \ell_1 m_1 n_1 \times \ell_2 m_2 n_2$. From a waveform modeling point of view, the second-order modes are just damped sinusoids, like the first-order modes. Spin-weighted spherical harmonics, rather than spheroidal harmonics, are commonly used for waveform extraction in numerical relativity [48]. In our analysis, the index k will belong to a set $I = \{\ell_1 m_1 n_1, \ell_2 m_2 n_2, \ldots \ell_i m_i n_i \times \ell_j m_j n_j \ldots\}$ containing all the indices of the QNMs present in the ℓm spin-2 spin-weighted spherical harmonic component. Then a ringdown waveform including both first- and second-order modes can be schematically written as

$$rh^{(2)}(t, \theta, \phi) = \sum_{\ell m} \sum_{k \in I} A_{k,\ell m} e^{-i(\omega_k t + \phi_{k,\ell m})} Y_{\ell m}, \quad (2)$$

where $A_{k,\ell m}$ and $\phi_{k,\ell m}$ are the amplitude and phase of the kth (linear or nonlinear) mode found in the ℓm spin-weighted spherical harmonic component. Note that $A_{\ell_1 m n, \ell_2 m}$ could be nonzero even if $\ell_1 \neq \ell_2$ because the spheroidal harmonic $S_{\ell_1 m}$ is not necessarily orthogonal to the spherical harmonic $Y_{\ell_2 m}$, even if $\ell_1 \neq \ell_2$ [48].

Because second-order QNM frequencies are sourced by first-order modes, their frequencies, amplitudes and phases are expected to obey the relationships [42–47]

$$\omega_{k_i \times k_j} = \omega_{k_i} + \omega_{k_j}, \quad (3a)$$

$$A_{k_i \times k_j, \ell_1 m_1} \propto A_{k_i, \ell_2 m_2} A_{k_j, \ell_3 m_3}, \quad (3b)$$

$$\phi_{k_i \times k_j, \ell_1 m_1} = \phi_{k_i, \ell_2 m_2} + \phi_{k_j, \ell_3 m_3} + \text{constant}. \quad (3c)$$

Second-order modes are a robust prediction of the perturbative expansion in general relativity. Other nonlinearities in the ringdown, such as the memory effect [49] or absorption-induced mode excitation [50], have previously been observed in simulations. However nonlinear QNMs have never been confidently identified until recently [51], with the exception of pioneering work by London et al. [45] using greedy fitting algorithms.

Second-order modes in merger simulations.—We have looked for the second-order modes in two sets of binary BH merger simulations. The first set consists of ultrarelativistic head-on collisions of equal-mass, nonspinning BHs with different boosts γ, similar to the sequences considered in

Refs. [52,53]. In this one-parameter family of solutions the amplitude of the linear mode increases with the boost parameter γ, so the amplitude of the second-order modes is also a monotonic function of γ. Axial symmetry allows us to simulate this problem in two dimensions with GRCHOMBO [54,55] by applying dimensional reduction [56–58], thus saving computational time and allowing for better accuracy relative to previous work [59]. As the quadratic modes are sourced by a product of two first-order modes, and quadratic contributions (proportional to $Y_{\ell_i m_i} Y_{\ell_j m_j}$) overlap with $Y_{\ell_i + \ell_j m_i + m_j}$, we will look for the $\ell_i m_i n_i \times \ell_j m_j n_j$ mode in the $\ell_i + \ell_j m_i + m_j$ ringdown waveform [43,45,47]. For head-on collisions, we will be fitting $r\Psi_4 = r\ddot{h}$ instead of h, and all of the reported amplitudes refer to $r\Psi_4$. In this case the 200 mode dominates the ringdown of the nonspinning remnant [52], so we focus mainly on the 200×200 mode in the $\ell m = 40$ waveform.

The second set of simulations consists of quasicircular mergers of binary BHs with different mass ratios from the publicly available SXS waveform catalog, simulated in $(3 + 1)$-dimensions with the spectral code SPEC [60]. Recent waveforms produced using Cauchy characteristic extraction [61–63] may improve the quality of our fits, but the relatively small set of publicly available waveforms does not adequately cover the relevant parameter space for our study. For quasicircular mergers the 220 and 330 modes are typically dominant (with their amplitudes depending on the mass ratio and spins of the binary), and we focus our search on (i) the 220×220 mode in the $\ell m = 44$ waveform, and (ii) the 220×330 mode in the $\ell m = 55$ waveform.

Identifying QNMs in a waveform can be challenging, partly because of their rapid decay; for nonspinning BHs, their quality factor is of order ~ 3 [14]. The search for subdominant modes, which decay faster, requires some care. Even if their inclusion yields smaller fit residuals, consistency checks are crucial to avoid overfitting. In this Letter we fit the waveforms by a linear combination of damped sinusoids, as in Eq. (2), using a least-squares fitting algorithm. The amplitude and phase of each mode are always free fitting parameters, while the complex QNM frequencies are either free or fixed depending on the mode, as shown in Fig. 1 and explained below.

We first try to find the second-order modes without assuming knowledge of their QNM frequencies, as follows. We consider the QNM frequencies as free fitting parameters, and we fit the waveform with a different number of QNMs as we vary the starting time of the fit t_{start}. If a fitted QNM returns a frequency that is consistent with a linear mode expected to exist in the waveform over a wide range of t_{start}, we assume that the mode is there. We then fix the frequency of that QNM (as calculated in BH perturbation theory) in our fit and we add more QNMs with free frequencies to search for additional modes. We iterate until
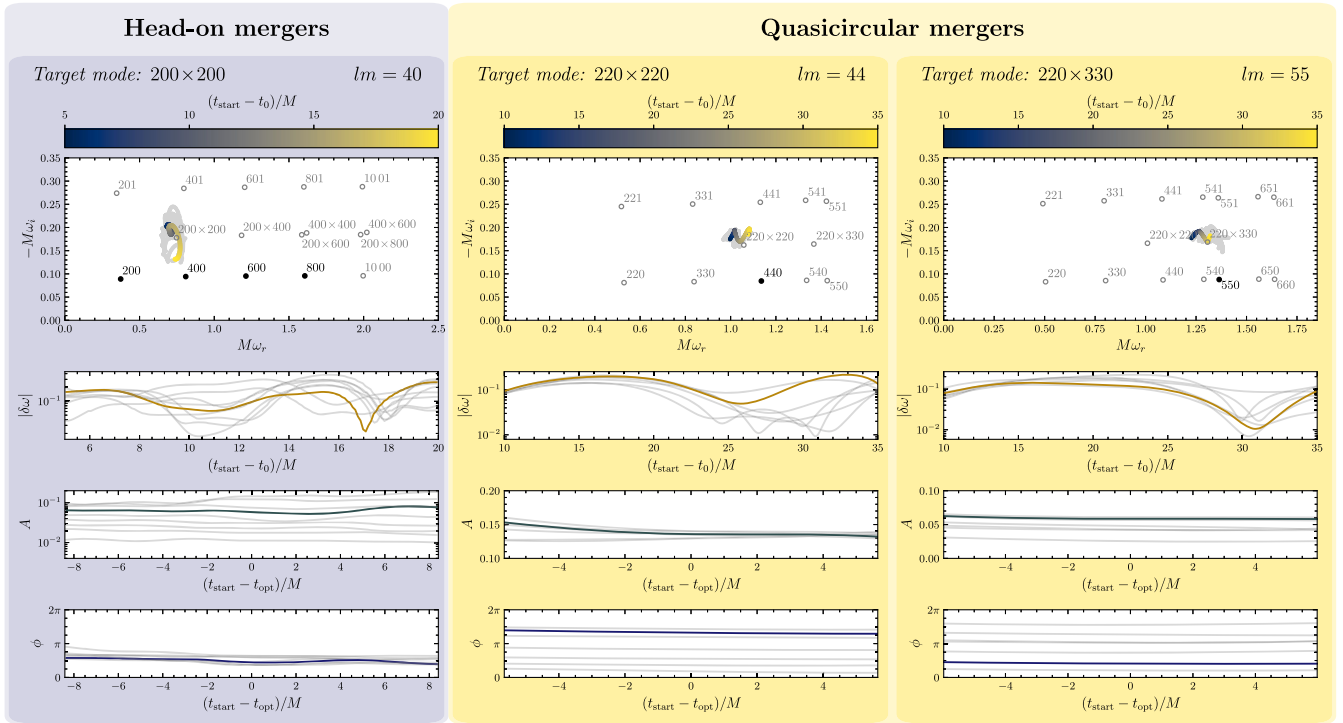
FIG. 1. Evidence for nonlinear effects in the ringdown. Left: search for the 200×200 mode in the $\ell m = 40$ multipole of ultrarelativistic head-on mergers; center: 220×220 mode in the $\ell m = 44$ harmonic of quasicircular mergers with low mass ratio $q \leq 1.5$; right: 220×330 mode in the $\ell m = 55$ harmonic of quasicircular mergers with $1.25 \leq q \leq 2$. We highlight in brighter colors the results for $\gamma = 1.5$ (left), $q = 1.22$ (the "SXS:BBH:0305" simulation, center) and $q = 1.88$ ("SXS:BBH:0403" simulation, right), while we plot the results for all other simulations in gray. Top row: search for the second-order mode frequency. We use a mode with a variable complex frequency in our fitting model to search for the expected second-order modes, and we use modes with fixed frequencies (black solid circles) to remove the contribution from linear modes when they are present. The color scale (top bar) represents different starting times of the fit. For quasicircular mergers, the labeled modes correspond to those of the remnant BH in the highlighted simulation. The location of the target mode for other simulations may be slightly different, because it depends on the remnant spin. Second row: fractional deviation $|\delta\omega|$ of the fitted complex frequency with respect to the expected second-order mode. Third row: amplitude of the second-order mode when t_{start} is varied across a window of length T_0 centered around the value of minimum $|\delta\omega|$, t_{opt}, and the second-order mode frequency is fixed to its expected value in the fitting model. Bottom row: same as the third row, but for the phase of the second-order mode.

we do not see returned frequencies that are consistent with any linear modes. For head-on high-energy mergers, we find a combination of the modes $200, 400 \ldots 10\,00$ in the $\ell m = 40$ waveform due to numerical contamination between modes. For the SXS waveforms, we only confidently identify the 440 mode in the $\ell m = 44$ multipole, and the 550 mode in the $\ell m = 55$ multipole (out of all possible linear modes). With these first-order modes identified, we use a fitting model that consists of all such modes (with *fixed* frequencies) to search for additional higher-order modes by adding one more damped exponential with free frequency. As shown in the top-row panels of Fig. 1, when we vary t_{start} relative to a reference time t_0 (defined to be the time of peak luminosity of the dominant $\ell m = 22$ multipole), the free mode hovers around the expected second-order mode frequency (from left to right: $\omega_{200\times200}$, $\omega_{220\times220}$, or $\omega_{220\times330}$, respectively). We do not expect the free mode frequency to converge exactly to the

expected frequency due to numerical noise and contamination from other effects (such as additional nonlinearities) in the waveform, especially for modes that decay significantly faster than the dominant mode. In the Supplemental Material [64], we show through a controlled experiment that a free frequency hovering near the target mode is the expected behavior in the presence of (small) unaccounted additional modes. We also searched for the 200×400 mode in the head-on simulations. The results (which are not as clean as those for the 200×200 mode, because 200×400 is subdominant) are shown in the Supplemental Material [64]. Having established the presence of nonlinear modes in the simulations, we now perform further checks to verify their physical nature.

Amplitude consistency check.—We cannot exclude *a priori* that the new mode we found is in accidental agreement with the expected second-order QNM frequency. A nontrivial consistency test requires that, in addition to the

frequency, the *amplitude* of the second-order modes should be consistent across different fitting ranges. To check this, we first look for the "optimal starting time," t_{opt}, for which the fractional deviation between the fitted and expected complex frequencies, i.e., $|\delta\omega| = \sqrt{[(\omega_r - \varpi_r)/\varpi_r]^2 + [(\omega_i - \varpi_i)/\varpi_i]^2}$, has a minimum. In the three cases of interest, $\varpi = \omega_{200\times200}$, $\omega_{220\times220}$, or $\omega_{220\times330}$, respectively. Then we assume that the mode exists, we fix the frequency to the expected value in our fitting model, and we check the consistency of the fitted amplitude. More explicitly, we check whether the recovered amplitude has an error smaller than 10% when t_{start} varies within a window of length T_0 centered around t_{opt}, where T_0 is the period of oscillation of the fundamental mode across all ℓm multipoles ($T_0 = T_{200}$ for head-on mergers, and $T_0 = T_{220}$ for inspirals). We choose this value of T_0 because it is at least two times larger than the period of the second-order mode that we are searching for. This threshold is further justified in the Supplemental Material [64] by studying the impact of the numerical noise in the simulations on the quantities of interest. Later times are excluded because the second-order mode falls below the numerical noise floor.

We find that all the waveforms we considered satisfy this requirement on the amplitude. We also checked that the amplitudes obtained from a model with free frequency are consistent with those where the frequency is fixed, albeit with larger fluctuations, as expected. Independently of the chosen t_{start}, we use the convention $A_{k,\ell m} \equiv A_{k,\ell m}(t_{\text{peak}})$. In other words, we take into account the known exponential time decay by extrapolating the fitted amplitudes back towards the peak of the dominant multipole.

Second-order amplitude dependence.—As a more stringent check, we can verify whether the recovered second-order mode amplitudes follow the dependence predicted in Eq. (3b) across different simulations. For each simulation, we extract the second-order mode amplitudes by taking the mean of the amplitude within the T_0 starting time window mentioned above. We extract the first-order mode amplitudes after $t_{\text{start}} - t_0 = 25M$, when nonlinearities and overtones have died out. We estimate the errors on the amplitudes as detailed in the Supplemental Material [64].

In Fig. 2 we plot the second-order mode amplitudes versus their first-order counterparts on a log-log plot. The data are consistent with a power-law dependence when the errors are taken into account. The slope of the fitted line for
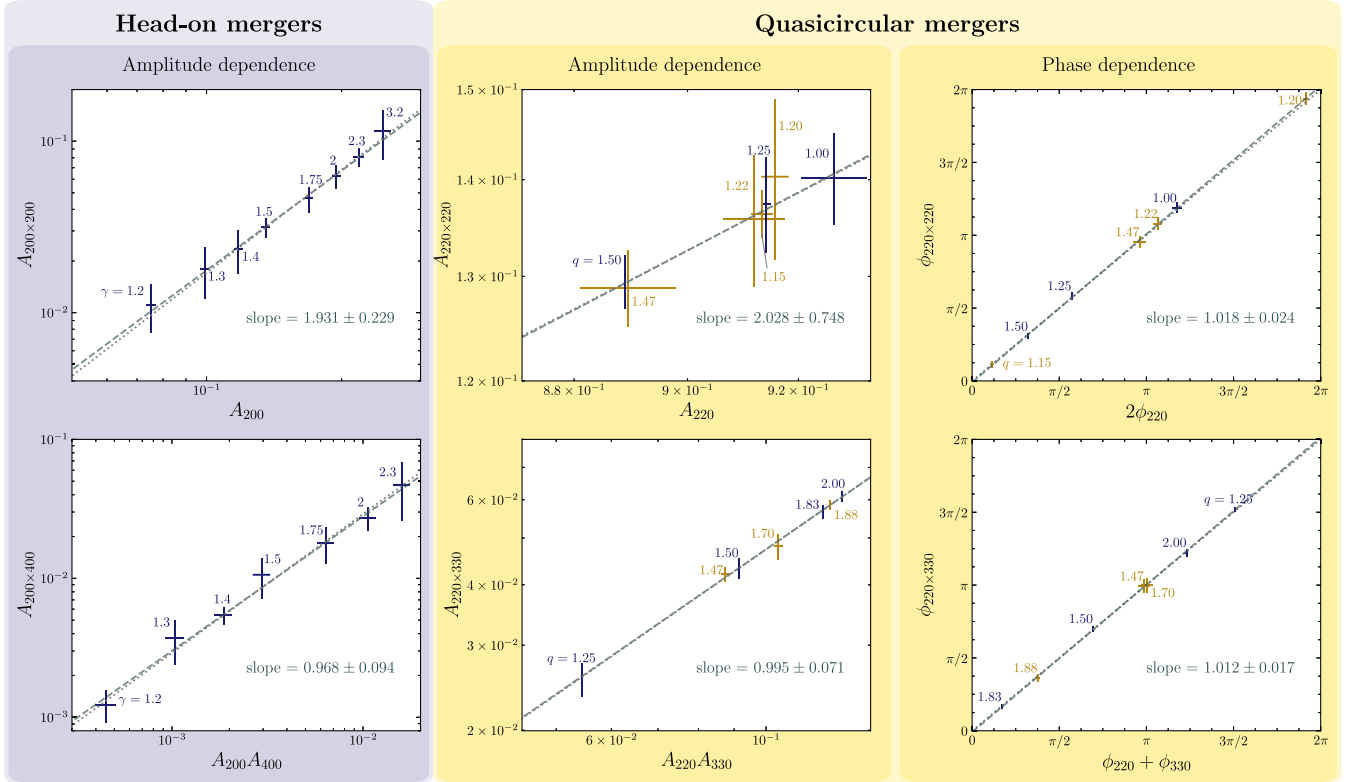

FIG. 2. Dependence of the second-order mode amplitude (left and middle columns) and phases (right column) on the amplitudes of the first-order modes sourcing them. The crosses are the amplitudes or phases extracted from simulations with different boost (left column) or mass ratio (center and right columns). The width and height of the crosses correspond to the errors. Blue crosses represent simulations where the two BHs are initially nonspinning, while golden crosses represent those with at least one spinning BH. The gray dotted line is the expected relationship between the first and second-order values with the slope fixed to either 1 or 2; the deep gray dashed line is a fit to the data with the slope unfixed. The phase dependence for head-on simulations is shown in the Supplemental Material [64].

$A_{200\times200}$ vs A_{200} (in the head-on waveforms) and $A_{220\times220}$ vs A_{220} (in the SXS waveforms) is found to be consistent with 2 within 1σ, as expected. Similarly, the slopes of the fitted lines for $A_{200\times400}$ vs $A_{200}A_{400}$ (for head-on waveforms) and $A_{220\times330}$ vs $A_{220}A_{330}$ (for SXS waveforms) are consistent with 1. Unsurprisingly, the 200×400 mode search results in head-on mergers are not as clean as the 200×200 results (see Supplemental Material [64]).

Because of numerical errors in the simulations, we can confidently identify the 220×220 mode only for SXS waveforms with mass ratio $q \leq 1.5$. Since q varies over a small range, the amplitudes of the 220 mode inferred from different simulations are similar to each other, and the amplitude of the 220×220 mode does not vary much across different simulations. For this reason the data points are relatively close to each other, and the error on the slope is larger than in the other cases we considered.

Phase consistency.—Similar to the amplitude tests, we can check the consistency of our fits with the fitted phases of the second-order modes. As shown in the bottom row of Fig. 1, the fitted phases of the second-order modes vary by less than $10\% \times 2\pi$ within the T_0 window.

Moreover, as the second-order modes are sourced by two linear QNMs, the relationship in Eq. (3c) between the phases of the modes should hold, modulo (possibly) a constant phase difference that can only be computed by a Green's function calculation. In the right column of Fig. 2 we show that the phases extracted from the SXS simulations follow the expected relationship. In the Supplemental Material [64] we show similar plots for head-on mergers. The error bars are larger, but the results are still consistent with expectations.

Conclusions.—We have shown that nonlinear QNMs are excited in simulations of comparable-mass BH binary mergers in quasicircular orbits, as well as in high-energy head-on BH collisions. The detectability of nonlinear QNMs may require next-generation detectors, and it will be addressed in future work. In any case, the presence of nonlinear modes demonstrates that nonlinearities must be taken into account in the modeling of GWs from binary BH mergers, and it suggests that they may play an important role during the violent merger phase. This has far-reaching consequences for our understanding of strong-field BH dynamics and for the observational BH spectroscopy program.

Note added.—While preparing this Letter, we learned that Mitman *et al.* conducted a similar study, whose results agree with ours [63].

[1] B. P. Abbott *et al.* (LIGO Scientific, Virgo Collaborations), Phys. Rev. Lett. **116**, 061102 (2016).

[2] E. Berti *et al.*, Classical Quantum Gravity **32**, 243001 (2015).

[3] L. Barack *et al.*, Classical Quantum Gravity **36**, 143001 (2019).

[4] N. Yunes, K. Yagi, and F. Pretorius, Phys. Rev. D **94**, 084002 (2016).

[5] V. Cardoso and L. Gualtieri, Classical Quantum Gravity **33**, 174001 (2016).

[6] E. Berti, K. Yagi, and N. Yunes, Gen. Relativ. Gravit. **50**, 46 (2018).

[7] E. Berti, K. Yagi, H. Yang, and N. Yunes, Gen. Relativ. Gravit. **50**, 49 (2018).

[8] V. Cardoso and P. Pani, Living Rev. Relativity **22**, 4 (2019).

[9] R. Abbott *et al.* (LIGO Scientific, VIRGO, KAGRA Collaborations), arXiv:2112.06861.

[10] F. Echeverria, Phys. Rev. D **40**, 3194 (1989).

[11] S. L. Detweiler, Astrophys. J. **239**, 292 (1980).

[12] K. D. Kokkotas and B. G. Schmidt, Living Rev. Relativity **2**, 2 (1999).

[13] O. Dreyer, B. J. Kelly, B. Krishnan, L. S. Finn, D. Garrison, and R. Lopez-Aleman, Classical Quantum Gravity **21**, 787 (2004).

[14] E. Berti, V. Cardoso, and C. M. Will, Phys. Rev. D **73**, 064030 (2006).

[15] E. Berti, V. Cardoso, and A. O. Starinets, Classical Quantum Gravity **26**, 163001 (2009).

[16] E. W. Leaver, Proc. R. Soc. A **402**, 285 (1985).

[17] E. W. Leaver, Phys. Rev. D **34**, 384 (1986).

[18] N. Andersson, Phys. Rev. D **51**, 353 (1995).

[19] E. Berti and V. Cardoso, Phys. Rev. D **74**, 104020 (2006).

[20] Z. Zhang, E. Berti, and V. Cardoso, Phys. Rev. D **88**, 044018 (2013).

[21] S. A. Hughes, A. Apte, G. Khanna, and H. Lim, Phys. Rev. Lett. **123**, 161101 (2019).

[22] H. Lim, G. Khanna, A. Apte, and S. A. Hughes, Phys. Rev. D **100**, 084032 (2019).

[23] N. Oshita, Phys. Rev. D **104**, 124032 (2021).

[24] H. Lim, S. A. Hughes, and G. Khanna, Phys. Rev. D **105**, 124030 (2022).

[25] L. London and S. A. Hughes, arXiv:2206.15246.

[26] A. Buonanno, G. B. Cook, and F. Pretorius, Phys. Rev. D **75**, 124018 (2007).

[27] E. Berti, V. Cardoso, J. A. Gonzalez, U. Sperhake, M. Hannam, S. Husa, and B. Brügmann, Phys. Rev. D **76**, 064034 (2007).

[28] M. Giesler, M. Isi, M. A. Scheel, and S. A. Teukolsky, Phys. Rev. X **9**, 041060 (2019).

[29] V. Prasad, A. Gupta, S. Bose, B. Krishnan, and E. Schnetter, Phys. Rev. Lett. **125**, 121101 (2020).

[30] M. Okounkova, arXiv:2004.00671.

[31] J. L. Jaramillo and B. Krishnan, arXiv:2206.02117.

[32] Y. Chen et al., arXiv:2208.02965.

[33] S. Bhagwat, M. Okounkova, S. W. Ballmer, D. A. Brown, M. Giesler, M. A. Scheel, and S. A. Teukolsky, Phys. Rev. D **97**, 104065 (2018).

[34] G. B. Cook, Phys. Rev. D **102**, 024027 (2020).

[35] P. Mourier, X. Jiménez Forteza, D. Pook-Kolb, B. Krishnan, and E. Schnetter, Phys. Rev. D **103**, 044054 (2021).

[36] E. Finch and C. J. Moore, Phys. Rev. D **103**, 084048 (2021).

[37] X. J. Forteza and P. Mourier, Phys. Rev. D **104**, 124072 (2021).

[38] E. Berti, V. Cardoso, and M. Casals, Phys. Rev. D **73**, 024013 (2006); **73**, 109902(E) (2006).

[39] S. A. Teukolsky, Astrophys. J. **185**, 635 (1973).

[40] R. J. Gleiser, C. O. Nicasio, R. H. Price, and J. Pullin, Classical Quantum Gravity **13**, L117 (1996).

[41] D. Brizuela, J. M. Martin-Garcia, and M. Tiglio, Phys. Rev. D **80**, 024021 (2009).

[42] K. Ioka and H. Nakano, Phys. Rev. D **76**, 061503(R) (2007).

[43] H. Nakano and K. Ioka, Phys. Rev. D **76**, 084007 (2007).

[44] E. Pazos, D. Brizuela, J. M. Martin-Garcia, and M. Tiglio, Phys. Rev. D **82**, 104028 (2010).

[45] L. London, D. Shoemaker, and J. Healy, Phys. Rev. D **90**, 124032 (2014); **94**, 069902(E) (2016).

[46] N. Loutrel, J. L. Ripley, E. Giorgi, and F. Pretorius, Phys. Rev. D **103**, 104017 (2021).

[47] J. L. Ripley, N. Loutrel, E. Giorgi, and F. Pretorius, Phys. Rev. D **103**, 104018 (2021).

[48] E. Berti and A. Klein, Phys. Rev. D **90**, 064012 (2014).

[49] L. Magaña Zertuche et al., Phys. Rev. D **105**, 104015 (2022).

[50] L. Sberna, P. Bosch, W. E. East, S. R. Green, and L. Lehner, Phys. Rev. D **105**, 064046 (2022).

[51] S. Ma, K. Mitman, L. Sun, N. Deppe, F. Hébert, L. E. Kidder, J. Moxon, W. Throwe, N. L. Vu, and Y. Chen, Phys. Rev. D **106**, 084036 (2022).

[52] U. Sperhake, V. Cardoso, F. Pretorius, E. Berti, and J. A. Gonzalez, Phys. Rev. Lett. **101**, 161101 (2008).

[53] J. Healy, I. Ruchlin, C. O. Lousto, and Y. Zlochower, Phys. Rev. D **94**, 104020 (2016).

[54] K. Clough, P. Figueras, H. Finkel, M. Kunesch, E. A. Lim, and S. Tunyasuvunakool, Classical Quantum Gravity **32**, 245011 (2015).

[55] T. Andrade et al., J. Open Source Softwaare **6**, 3703 (2021).

[56] F. Pretorius, Classical Quantum Gravity **22**, 425 (2005).

[57] W. G. Cook, P. Figueras, M. Kunesch, U. Sperhake, and S. Tunyasuvunakool, Int. J. Mod. Phys. D **25**, 1641013 (2016).

[58] M. Shibata and H. Yoshino, Phys. Rev. D **81**, 104035 (2010).

[59] T. Helfer et al. (to be published).

[60] M. Boyle et al., Classical Quantum Gravity **36**, 195006 (2019).

[61] J. Moxon, M. A. Scheel, and S. A. Teukolsky, Phys. Rev. D **102**, 044052 (2020).

[62] J. Moxon, M. A. Scheel, S. A. Teukolsky, N. Deppe, N. Fischer, F. Hébert, L. E. Kidder, and W. Throwe, arXiv:2110.08635.

[63] K. Mitman et al., following Letter, Phys. Rev. Lett. **130**, 081402 (2023).

[64] See Supplemental Material at http://link.aps.org/supplemental/10.1103/PhysRevLett.130.081401 for additional results, a description of the simulations used, error estimates, and controlled experiments to test the mode-fitting criteria.

[65] L. C. Stein, J. Open Source Softwaare **4**, 1683 (2019).

[66] J. D. Hunter, Comput. Sci. Eng. **9**, 90 (2007).

[67] C. R. Harris et al., Nature (London) **585**, 357 (2020).

[68] D. Stanzione, J. West, R. T. Evans, T. Minyard, O. Ghattas, and D. K. Panda, in Practice and Experience in Advanced Research Computing, PEARC'20 (Association for Computing Machinery, New York, 2020), pp. 106–111.

[69] http://www.tacc.utexas.edu.